ORIGINAL ARTICLE

Evaluation of the effect of nanosilica and recycled fine aggregate in Portland cement rendering mortars

Avaliação do efeito da nanossílica e agregado miúdo reciclado em argamassas de reboco de cimento Portland

Geannina Terezinha dos Santos Lima[a]
Alessandra Zaleski[a]
Luís Urbano Durlo Tambara Júnior[a]
Janaíde Cavalcante Rocha[a]
Fernando Pelisser[b]
Philippe Jean Paul Gleize[b]

[a]Universidade Federal de Santa Catarina – UFSC, Laboratório de Valorização de Resíduos e Materiais Sustentáveis – ValoRes, Departamento de Engenharia Civil, Florianópolis, SC, Brasil

[b]Universidade Federal de Santa Catarina – UFSC, Laboratório de Aplicações de Nanotecnologia em Construção Civil – LabNANOTEC, Departamento de Engenharia Civil, Florianópolis, SC, Brasil

Abstract: This paper evaluated the incorporation of nanosilica (NS) in rendering mortars produced with recycled fine aggregate (RFA). Initially, a study was carried out on cementitious pastes, replacing Portland cement with NS at levels of 0%, 0.4%, 0.6%, 0.8%, and 1.0%. The samples were submitted to scattering, rheology, calorimetry, x-ray diffraction (XRD), Fourier transform infrared spectroscopy (FTIR), and compressive strength analysis at 28 days. The results demonstrated that the pastes with 0.4% NS and 0.6% NS presented an increase in strength of 55% and 58%, respectively, due to a greater formation of calcium silicate hydrate (C-S-H), when compared with the reference paste. From that, the RFA samples were produced, replacing Portland cement with 0% NS, 0.4% NS, and 0.6% NS. At 28 days, mechanical performance, microstructure, and durability were evaluated by means of flexural strength and compression, scanning electron microscopy (SEM), dynamic elasticity module, and water absorption by capillarity. From the results, it was concluded that the RFA samples with 0.4% NS resulted in the optimal nanosilica content, increasing compressive strength values and reducing the sorptivity, in relation to the other mixtures. The SEM images suggest that NS reacted with portlandite formed of the cement hydration, improving the microstructural development of the samples.

Keywords: Portland cement paste, rendering mortars, fine recycled aggregate, nanosilica, rheology.

Resumo: Esta pesquisa teve como objetivo avaliar a incorporação da nanossílica (NS) em argamassas de reboco produzidas com agregado fino reciclado (RFA). Inicialmente, foi realizado um estudo em pastas cimentícias substituindo o cimento Portland por NS nos teores de 0%, 0,4%, 0,6%, 0,8% e 1,0%. As amostras foram submetidas a análises de espalhamento, reologia, calorimetria, difração de raios X (DRX), espectroscopia de infravermelho por transformada de Fourier (FTIR) e resistência à compressão aos 28 dias. Os resultados demonstraram que as pastas com 0,4% NS e 0,6% NS apresentaram aumento de resistência de 55% e 58%, respectivamente, devido à maior formação de silicato de cálcio hidratado (C-S-H), quando comparada à pasta de referência. Diante disso, foram produzidas as amostras de RFA, substituindo o cimento Portland por 0% NS, 0,4% NS e 0,6% NS. Aos 28 dias, o desempenho mecânico, a microestrutura e a durabilidade foram avaliados por meio da resistência à flexão e compressão, microscopia eletrônica de varredura (MEV), módulo de elasticidade dinâmico e absorção de água por capilaridade. A partir dos resultados, concluiu-se que as amostras de RFA com 0,4% NS resultaram no teor ótimo de nanossílica, produzindo um aumento na resistência à compressão e redução na sorptividade de água, em relação às demais misturas. As imagens de MEV sugerem que NS reagiu com a portlandita formada a partir da hidratação do cimento, resultando em um enchimento eficiente dos poros do RFA, melhorando o desenvolvimento microestrutural das amostras.

Palavras-chave: pasta de cimento Portland, argamassa de revestimento, agregado fino reciclado, nanossílica, reologia.

G. T. S. Lima, A. Zaleski, L. U. D. Tambara Júnior, J. C. Rocha, F. Pelisser, and P. J. P. Gleize

1 INTRODUCTION

The construction industry is one of the most important economic sectors worldwide, as it drives the economy in developed and underdeveloped countries. However, the nature of its activity has serious environmental impacts. In addition to the consumption of large quantities of natural resources and the emission of polluting gases into the atmosphere, this sector is responsible for the production of construction waste.

According to Akhtar and Sarmah [1], the countries that generate the largest amounts of construction and demolition (C&D) waste are China (1,020 million tons per year), India (560 million tons per year), and the United States (519 million tons per year). Of these countries, only the United States has recycling and reuse strategies, determined by the United States Environmental Protection Agency (USEPA) [2]. In Brazil, the estimated production of this waste is over 70 million tons per year, and although the country has recently implemented new laws for recycling waste, the recovery rate is still minimal [1].

In this context, the use of C&D waste as recycled aggregate in construction materials is one of the alternatives for proper disposal and reducing the consumption of natural resources. The recycled aggregate is produced in both fine and coarse particles. According to Tabsh and Abdelfatah [3], fine aggregate (RFA) particles generally have large amounts of hydrate cement and plaster in their physical composition. The fine particles (grains smaller than 15 μm in diameter) are one of the major problems encountered in the recycling process of C&D waste, as they are usually sent to stabilization ponds, generating more waste. Recycled coarse aggregates (RCA) are more easily used in the production of concrete and bases and sub-bases in paving areas.

RFA is most often used in plastering and laying mortars, however it has inferior physical-mechanical properties and durability than the material constituted with natural aggregate [4]–[6]. The finer particles of the recycled aggregate have an old interfacial transition zone due to the presence of glued mortar or cement paste that surrounds the aggregate. In addition, it contains tiny pores of adherent mortar, continuous cracks, and cracks developed within the aggregate because of the crushing process. Due to these characteristics, when the recycled aggregate is incorporated into the concrete or mortar, it can cause a weak adhesion between the new cement paste and the recycled aggregate and, therefore, decrease the mechanical properties and increase the water absorption [7].

The microstructure of the recycled aggregate has two transition zones; one is the new transition zone located between the recycled aggregate and the new matrix, and the other is the old transition zone located between the recycled aggregate and the old adhering mortar. Thus, the mechanical performance of the recycled aggregate is a result of the performance of both transition zones, which significantly influences the strength property [8]. These transition zones form a very weak link and a strength limitation in the recycled aggregate, acting as a barrier for the mechanical properties. However, the appearance of cracks will first form near the transition zone. The porous nature of the interfacial transition zone of the recycled aggregate may cause a reduced modulus of elasticity and lower strength in the surface area of mortar and concrete [9].

Therefore, there is an increasing search to incorporate new materials in mortars and concrete with recycled aggregates, to improve their physical-mechanical properties. According to Wang et al. [10], pozzolanic materials such as fly ash, blast furnace slag, silica fume, and metakaolin can react with calcium hydroxide ($Ca(OH)_2$) to generate hydrated calcium silicates (C-S-H), effectively reducing the porosity of the RFA and RCA, creating a denser transition zone, and thus improving the microstructure and the mechanical properties of mortars and concretes with recycled aggregate.

Studies have been made to evaluate the effect of nanoparticles in cement composites in an effective way to modify the mechanisms of hydration in cement pastes [11]–[19]. NS shows that modifies the structure of C-S-H gel resulting from C_3S hydration due to the pozzolanic reaction between NS and portlandite [17]. In other hand, it reduces the C_3A dissolution rate and the consumption of gypsum, hindering the precipitation of its hydrates, arising from the adsorption of NS on the surface of C_3A [18]. NS provides a reduction in the mixture's hardening time, increases mechanical and durability properties and decreases the water permeability of the Portland cement-based materials due to the filler effect and the reaction with $Ca(OH)_2$ which forms a denser structure [14], [20].

A recent work that evaluated the performance of NS in concrete with recycled coarse aggregate [12] showed that with 0.5% incorporation of NS a reduction of 14% in compressive strength, 10% in flexural strength, and 37% in elasticity modulus when compared with the mixture with natural aggregate (NA). However, with 1.5% NS, the increase in compressive and flexural strength for mixtures with RCA was 6% and 4%, respectively, in relation to NA. This is due to the pozzolanic activity reactions and the acceleration of the cement paste hydration rate, resulting in a stronger bond between paste-aggregate [12]. Tobón et al. [21] produced mortars with cement substitutions for NS (up to 10%) and added SP for the correction of fluidity. The NS showed that it has an important role in the refinement of the pores,

decreasing the total volume of pores and their diameters, which increased mechanical strength and decreased the absorption rate and total water absorption in the mortars.

The few and scarce studies evaluating the incorporation of NS with recycled fine aggregates show distinct results as a contribution, as mentioned above. However, NS can show an important material to improve the poor performance of mortars made with RFA, especially in aggressive environments or when under mechanical stress. Therefore, the objective of this study was to investigate the influence of NS in the substitution of Portland cement in pastes and mortars composed with RFA, compared with a control mortar.

Initially, the fresh and hardened properties of cementitious pastes were analyzed with the incorporation of NS in the contents of 0%, 0.4%, 0.6%, 0.8%, and 1.0%. The pastes were subjected to rheology, mini-slump, and calorimetry tests in their fresh state, and at 28 days the formation of hydration products and compressive strength were evaluated. After evaluating the incorporation of NS in cementitious pastes, optimum levels of NS were selected to evaluate the mechanical properties, microstructure, and durability of laying and rendering mortars with RFA.

2. EXPERIMENTAL PROGRAM

2.1 Materials

The Portland cement (PC) used was type CPV-ARI, according to NBR 16697 [22], equivalent to Type III by ASTM C150 [23], with a Blaine specific surface area of 440 m^2/kg and a specific gravity of 3.12 g/cm^3. The chemical composition of the cement was determined by X-ray fluorescence (XRF) and is presented in Table 1. Two types of additives were used: SP based on naphthalene sulfonate and Hydroxypropyl Methylcellulose (HPMC), a cellulose ether (Methocel™). The purpose of the HPMC is to improve the adhesion of the particles, as well as retain the water in the mixture, avoiding possible cracks in the curing process in the sample. The SP, on the other hand, allows for excellent fluidity and cohesion, improving the workability of the mixture. A powdered NS from the brand AEROSIL 200 (particle size 12 nm) was used, with 99.8% SiO_2, a surface area of 175-225 m^2/g, and a density of 2.20 g/cm^3. The X-ray diffraction (XRD) of NS (Figure 1) was performed in a MiniFlex II diffractometer equipment, using a 2θ range of 5–70° with a step of 0.02° and an accumulation time of 30 s. It can be observed that NS presented a predominant amount of amorphous phase, with a halo between 10-40° 2θ.
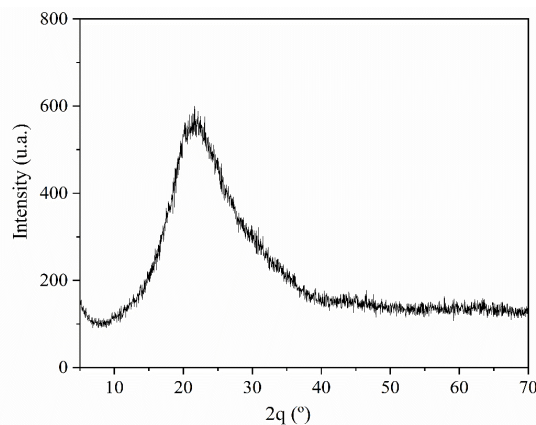
Figure 1. X-ray diffractogram of NS.

Table 1. Chemical composition of Portland cement.

Composition	SiO$_2$	Al$_2$O$_3$	Fe$_2$O$_3$	CaO	MgO	SO$_3$	LoI[a]	IR[b]
wt (%)	17.69	4.09	3.08	67.81	4.11	4.65	4.68	1.04

[a]Loss on ignition; [b]Insoluble residue

The characterization of the RFA to produce mortars was carried out through the particle size tests, fines content <75 µm, specific gravity, and water absorption following NBR 7211 [24], NBR NM 46 [25], NBR 16916 [26], respectively. RFA presented fineness modulus equal 2.25, 11.55% of particle size under 75 µm, mean particle size (D50) of 1.80

G. T. S. Lima, A. Zaleski, L. U. D. Tambara Júnior, J. C. Rocha, F. Pelisser, and P. J. P. Gleize

mm and (D90) 90% less than 10.90 mm, density of 2.60 g/cm^3 and 7.12% of water absorption. The Brazilian normal sand, according to NBR 7215 [27], was used in the control mortar (REF) with 25% of each fraction of coarse (1.20 mm), medium coarse (0.60 mm), medium fine (0.30 mm), and fine (0.15 mm) proportion. The granulometric curve of RFA and normal sand are presented in Figure 2.
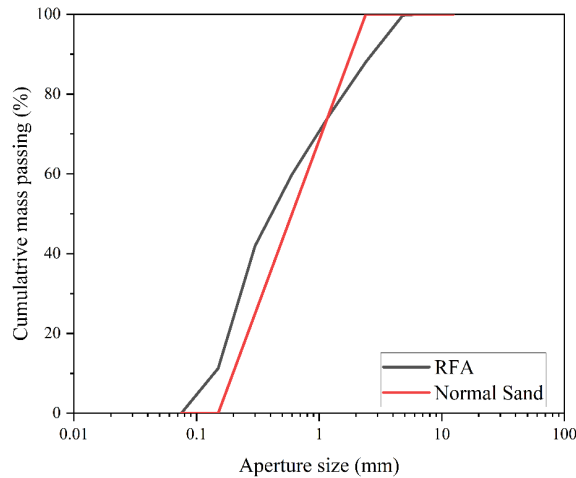
Figure 2. Particle size distribution of RFA and normal sand.

2.2. Paste preparation and hydration product characterization

The Portland cement was replaced by NS in the following proportions: 0%, 0.4%, 0.6%, 0.8%, and 1.0%, by weight of cement. To produce pastes a water/binder (binder = cement + NS) ratio of 0.45 was adopted. For all mix proportions, enough SP was added to achieve a spread of 90 ± 20 mm in the mini-slump test. Furthermore, the HPMC content was fixed at 0.003%. Both additives were added over the binder weight.

The cement pastes were produced in a mixer at 10,000 rpm, according to the following steps: (i), dry material (PC and NS) were previously homogenized; (ii) dry material were added to 50% water and mixed for 1 min; (iii) SP was manually mixed with 25% water, being subsequently inserted into the sample and mixed for 40 s; (iv) the mixer was stopped to scrape down any material found in the mixer impeller and/or container wall, during 20 s. (v) the HPMC and the rest of the water (25%) were added to the paste mixing for 1 min; (vi) lastly, the paste was mixed for another 2 min. Immediately after mixing, the fresh state and calorimetry tests were started.

The fluidity of the fresh cement paste was determined by the mini-slump test, using a mold proportional in size to the standard cone (small/standard = 0.19), recording the average of two spread measurements [28], [29]. Table 2 presents the composition of the pastes produced, nomenclature of the mixture is given by replacement content of NS, by weight of cement.

Table 2. Sample composition of the cement pastes per 100 g of binder.

Mixture	w/b	PC (%)	NS (%)	HPMC (%)	SP (%)
0NS	0.45	100.0	0.0	0.003	0.2
0.4NS	0.45	99.6	0.4	0.003	0.3
0.6NS	0.45	99.4	0.6	0.003	0.4
0.8NS	0.45	99.2	0.8	0.003	0.5
1.0NS	0.45	99.0	1.0	0.003	0.6

For each composition, six cylindrical specimens of 25 × 50 mm (diameter x height) were cast for a compressive strength test at 28 days. The specimens were demolded after 24 h and kept in relative humidity of 100% at 23 ± 2 °C until testing.

The rheological properties of the paste investigated were performed 15 min after the water/binder contact using a Haake Mars III rheometer (Thermo Scientific), with a maximum torque of 200 N.mm and a maximum rotation speed of 1500 rpm. The geometry used was the coaxial of concentric cylinders, using a rotor with a diameter of 24 mm and a gap of 5 mm, with a

controlled temperature of 23 ± 2 °C. The rheological test was performed according to the shear process used by Azevedo et al. [30]. A pre-shear at 100 s^{-1} was applied for 1 min to create a uniform condition before testing. Then, two shear cycles were performed by two ramps (ascending and descending). In the first curve (ascending) a shear rate from 5 s^{-1} to 100 s^{-1} in 90 s was applied. The second (descending) curve started from the point 100 s^{-1} and returned to 5 s^{-1} in another 90 s. The test was performed on two samples per mixture and it was used Bingham model (Equation 1) [31], [32].

$$\tau = \tau_{\circ} + \eta_{pl}.\gamma \tag{1}$$

Where = τ_o is the yield stress (Pa), η_{pl} is the plastic viscosity (Pa s) and γ is the shear strain rate (1/s).

The hydration heat release of each Portland cement paste was measured using an isothermal calorimeter (TAM Air, TA Instruments) to assess the effect of NS on the hydration kinetics of cement. The test lasted 72 h at a temperature of 23 °C ± 1, for approximately 15 g of fresh paste, starting 5 minutes after the first water contact.

To stop the hydration process, at 28 days of hydration, some pieces of paste were grounded (particle size under 45 μm) and mixed for 3 min with acetone, filtered, and dried in a desiccator to constant weight for subsequent microstructural analysis, this has been reported to be the best method to preserve the microstructure of the samples, according to [17]. XRD tests were conducted using an X' Pert Pro (PANalytical) with CuKα radiation and a wavelength of 1.5408 Å. The scanning range and step size were respectively 7–70° 2θ and 0.02° 2θ. FTIR test was performed using the JASCO FT IR-4200 spectrometer. Micropellets were prepared to mix paster powder with potassium bromide (KBr) in the proportion of 1:100 and analyzed at frequencies of 400 cm^{-1} to 4000 cm^{-1}, with a scan number of 32 and a resolution of 16 cm^{-1}. NBR 7215 [27], equivalent to ASTM C39 [33], was used to determine the compressive strength of cement pastes using an Instron Universal Testing Machine, also at 28 days.

2.3. Mortar preparation and test methods

Mortars were prepared with the proportions given in Table 3. Initially, a water/binder (w/b) ratio was fixed at 0.48. Then, the binder: RFA ratio was defined as 1:3 by weight. The SP was dosed to obtain a spread of at least 260 ± 10 mm in the flow table test, while the HPMC content was fixed at 0.003%. The use of an addictive was also aimed to improve the dispersion of nanosilica in the cement matrix [34]. Both additives were incorporated into the total weight of the binder.

The recycled aggregate was used in a saturated-surface-dry (SSD) state. The mixing procedure was based on NBR 16541 [35] and produced in a mortar planetary mixer with a capacity of 5 L. The workability of the mixes was evaluated through the flow table test according to NBR 13276 [36] and SP was added to reach the same slump for all the samples (260±10 mm). Table 3 presents the detailed composition of the mixes produced. A blank mortar (REF) was made with standardized sand to compare with RFA with the same binder: sand of 1:3 by weight.

Table 3. Detailed composition of the mortar mixes per 100 g of binder.

Mixture	w/b	PC (g)	NS (g)	HPMC (%)	SP (%)	Regular Sand (g)	RFA (g)	Slump (mm)
REF	0.48	100.0	0.0	0.003	0.5	300.0	0.0	261.0
0NS	0.48	100.0	0.0	0.003	1.0	0.0	300.0	256.0
0.4NS	0.48	99.6	0.4	0.003	1.8	0.0	300.0	255.5
0.6NS	0.48	99.4	0.6	0.003	1.9	0.0	300.0	251.8

The compressive, flexural, and dynamic elastic modulus (E_d) tests were performed on mortars prepared in prismatic molds (40 × 40 × 160 mm). Cylinders of 50 × 100 mm (diameter x height) were cast for the tests on the capillary water absorption and sorptivity test. All tests were performed at 28 days of cement hydration. After 24 h, the specimens were demolded and cured in a humidity chamber (temperature of 23 °C and 95% relative humidity) until the respective test age.

The capillary water absorption test was performed according to NBR 9779 [37]. The compressive strength of the mortar was determined on the halves of the prisms after fracture of the flexure specimens, according to ASTM C 349 [38] and ASTM C 348 [39]. The dynamic modulus of elasticity (Ed) test was conducted using Sonelastic (ATCP Physical Engineering) impulse equipment according to ASTM-E1876 [40].

After the compressive tests, pieces of broken specimens of some mixes were collected. The samples were gold-coated, and SEM images were obtained using a JSM-6390LV (JEOL) microscope operating at 20 kV.

G. T. S. Lima, A. Zaleski, L. U. D. Tambara Júnior, J. C. Rocha, F. Pelisser, and P. J. P. Gleize

4. RESULTS AND DISCUSSION

4.1 Portland cement pastes

4.1.1 Rheological test

Figure 3 shows that the paste fluidity declined with the rising of NS dosage, requiring increment of SP content. This is due to the greater surface area that NS presents when compared with Portland cement [41]. Additionally, the higher SP demand is provided by the higher amount of water retained as result of the agglomeration of nanoparticles in the mixture that contributes to the workability decrease in the cement pastes with NS [31].
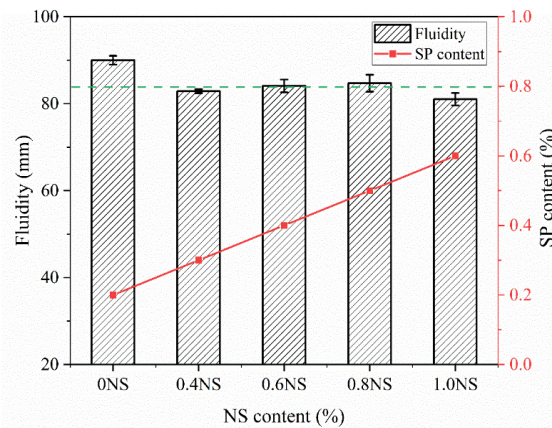
Figure 3. Influence of NS on the fluidity of the cement pastes.

The purpose of the rheometry test was to obtain the influence of NS in the yield stresses and viscosities of cement pastes. In the first step, the flow curves of the pastes were analyzed, considering the ascending and descending cycles and a heterogeneity of the results was observed.

The shear stress (τ) was obtained for 2nd descending shear rate that presented a consistent and repeatable rheological parameter (as observed in the Figure 4a). Figure 4b shows the preliminary analysis carried out for the rheology test. To obtain the values of yield stress and viscosity, the Bingham model was chosen due to the liner proportion between shear rate and stresses. Then, the yield stress for each paste was obtained from the respective flow curves. The shear stress versus shear rate and viscosity versus shear rate plots were generated to compare the shear stress and viscosity of the samples.
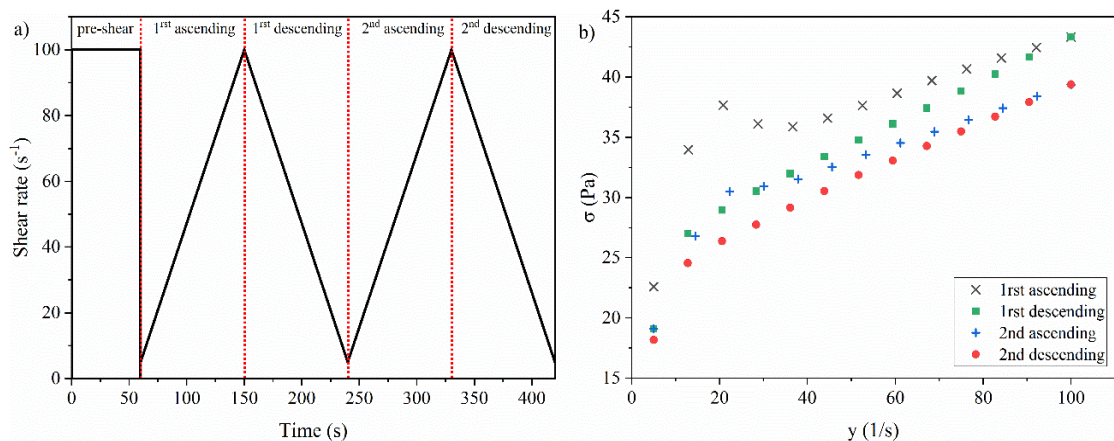
Figure 4. Shear process analyzed from the ascending and descending cycle.

In Table 4, the yield stress (τ_0) and plastic viscosity (η) parameters of the pastes are presented. It is noted that the yield stress of the NS pastes was higher than the value observed in the reference paste (11.50 Pa), with a maximum value of 24.70 Pa found for 0.4% NS. The mixtures 0.4% NS, 0.6% NS, 0.8% NS, and 1.0% NS showed an increase in the minimum tension of 116%, 15%, 29%, and 75%, respectively, in relation to the reference paste (0NS). The use of finer materials (NS) promotes an increase in the minimum necessary tension to be applied to allow the paste to flow.

For Berra et al. [31], the use of SP reduces the yield stress and the plastic viscosity of pastes containing NS. This is due to the development of dispersive forces in the mixture (electrostatic repulsion and the steric effect) caused by the adsorption of the SP on cement and NS particles, resulting in a better deflocculation of the paste particles. García-Taengua et al. [16] found similar results in the yield stress in mortars containing NS, concluding that variations in the SP dose significantly influence the yield stress and that the greater the amount of SP (0.9%), the lower the stress of flow for mortars with up to 3.5% NS. In this work, as there was an increase in SP content (0.4%, 0.5%, and 0.6%), the yield stress gradually increased (0.6% NS, 0.8% NS, and 1.0% NS), except for 0.4% NS paste with 0.3% SP.

Table 4. Rheological parameters for cement pastes.

Mixtures	0NS	0.4NS	0.6NS	0.8NS	1.0 NS
τ_0 (Pa)	11.50	24.70	13.20	14.80	20.00
η (Pa·s)	0.28	0.33	0.24	0.25	0.34

In general, the increase in the NS and SP content together implies an increase in the yield stress of the pastes. For the viscosity parameter, the paste with 1.0% NS showed a superior result when compared with the other mixtures, reaching an increase of 24% in comparison to the reference paste (0NS). The 0.4% NS paste had a 20% increase, while the 0.6% NS and 0.8% NS pastes had reductions in viscosity of 14% and 11% when compared with 0NS. The results of plastic viscosity showed a tendency similar to yield stress when analyzing the effect of SP in pastes with NS.

Figure 5a shows the results of the shear stress by the shear rate of the pastes with their respective levels of NS. The results indicated that the Bingham model can adequately describe the data. From the flow curves, it is possible to observe that the 0.4% NS paste presented higher shear stress, as well as a greater increase in flow stress (Table 5), than the other pastes. This may have occurred due to the lower dosage of SP needed to achieve the desired consistency in this case. In addition, the shear stress behavior of pastes with 0.6% NS and 0.8% NS was similar to the reference paste, as well as obtaining lower yield stress (Table 5). For Flores et al. [42] the higher shear stress value of NS pastes is caused by increased surface friction. Since NS has a greater specific area that retains part of the water in the mixture, the availability of water decreases and hinders the lubrication of the nanomaterials particles [43], [44].
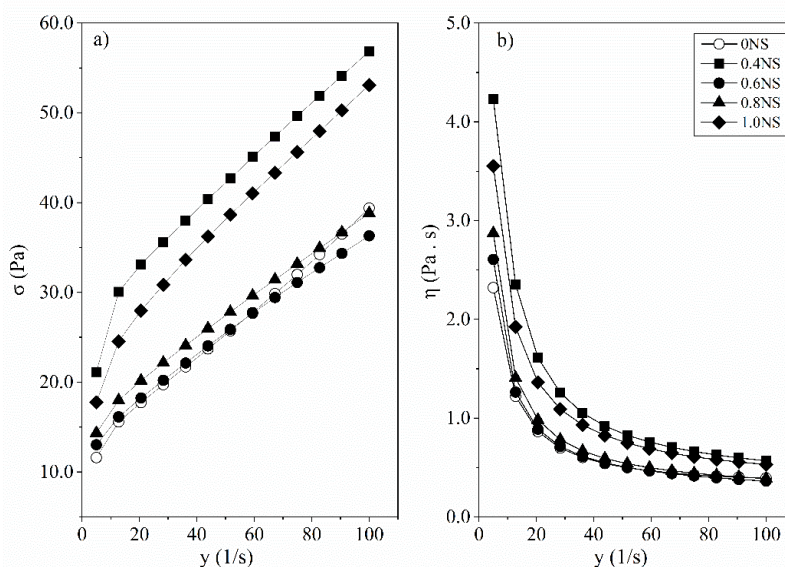
Figure 5. (a) Shear stress *vs* shear rate deceleration (b) Viscosity *vs* shear rate deceleration

Figure 5b shows the results of the viscosity by the shear rate of the pastes with their respective levels of NS. It is possible to observe that the substitutions of 0.4% and 1.0% of cement by NS increased the viscosity of the pastes. The viscosity flow x shear rate curve for mixtures with 0.6% NS and 0.8% NS presented the same behavior as the reference paste (0NS). According to Azevedo et al. [30], nanomaterials absorb water and fill voids in cement paste, resistance to flow increases, and consequently, the viscosity values of pastes with the addition of nanomaterials tend to be higher than the reference paste, further contributing to improving the cohesion of Portland cement paste.

The analysis of the rheological parameter revealed that the substitution of cement by NS at 0.6% was the paste that achieved the best results. Therefore, the lowest flow tension was reached, allowing greater fluidity and less apparent viscosity, which led to easier paste flow.

4.1.2 Hydration of cement pastes

The heat flow and total heat release of the pastes are shown in Figure 6. The presence of NS accelerated the cement hydration, behavior confirmed by other authors [16], [42]. Portland cement hydration was divided into four stages: the initial period, dormant period, acceleration period, and retardation period. Two maximum heat flows were observed, the first is attained after the beginning of the acceleration period and the second during the deceleration period [45]. The first peak represents the formation of C-S-H gel and alite dissolution while the second peak is related to the formation of ettringite and the sulfate depletion [45]–[47].

Table 5 presented the dormant period, the maximums peak information, and the total heat release at 65 h for all the samples. According to Figure 6a, the reference paste with 1.0% NS was the first mixture to reach a maximum heat flow (6.44 mW/g) at a time of 18.56 h, 8 hours early than the reference paste that reached a maximum heat flow (5.43 mW/g) at 26.68 h. It is also noted that among the pastes containing NS, the lower content of NS tends to increase the dormant period and the heat flow. 0.4% NS reached a similar 1[rst] peak heat flow than the reference (5.41 mW/g), however, the time was accelerated around 7 hours (20.70 h).

Flores et al. [42] state that the increased hydration for pastes containing NS was mainly associated with the hydration of tricalcium silicate (C_3S). The increase in acceleration can be attributed to the nucleation effect of the NS particles, which is associated with the reduction of the induction period [16]. It should also be taken into account that, due to the greater surface area of the nanomaterials, the amount of free water in the mixture is reduced, which results in an increase in the concentration of alkaline ions, contributing to the acceleration of the initial hydration reactions [44], [48].
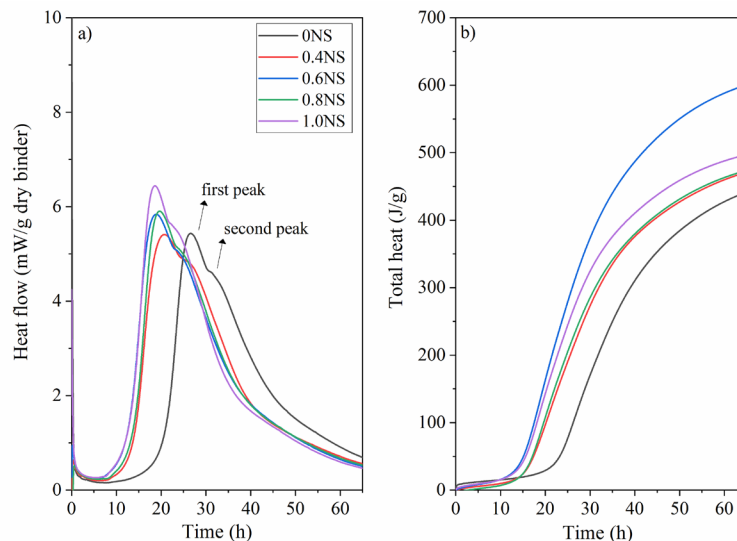
Figure 6. Effect of NS on cement pastes on isothermal calorimetry results. a) heat flow and b) total heat released.

Figure 6b shows the total heat release for all mixtures. It was possible to observe a significant increase in the total heat released of 8%, 13%, 8%, and 14% in pastes with 0.4% NS, 0.6% NS, 0.8% NS, and 1.0% NS, respectively, when compared with the reference paste. This indicates an increase in the formation of the hydrated phases of the NS pastes compared to the mixture with Portland cement [16].

Table 5. Calorimetric parameters for cement pastes with NS.

Cement pastes	Dormant period (h)	Maximum 1 st peak (h)	1 st peak heat rate (mW/g)	Maximum 2 nd peak (h)	2 nd peak heat rate (mW/g)	Cumulative heat evolution at 65 h (J/g)
0NS	18.82	26.68	5.43	32.36	4.47	441.82
0.4NS	11.80	20.70	5.41	26.50	4.80	471.29
0.6NS	9.95	18.87	5.84	24.20	5.01	600.74
0.8NS	10.86	19.62	5.90	24.97	4.99	473.93
1.0NS	9.78	18.56	6.44	23.82	5.44	497.33

4.1.3 XRD analysis

The XRD diffractograms of the mixtures at 28 days are shown in Figure 7. For portlandite phase, the peak intensity at 18.1 º (2Θ) related to the 001 reflections increased but the intensity at 34.1 º (2Θ) related to the 101 reflections decreased for pastes made with NS, resulting in a higher R index for samples containing nanosilica. This is associated with a portlandite structure with a lower diameter than reference pastes [49].

The peak close to 30 º (2Θ), referring to the C_3S and C_2S phases, showed a constant reduction of intensity for the 0.4NS, 0.6NS, and 0.8NS pastes, resulting in a higher hydration degree for these compositions. However, 1.0NS presented similar peaks intensities to the reference, indicating that the degree of reaction reduces in pastes with levels above 0.8% of nanosilica, probably related to poor dispersion of nanosilica in the matrix at high contents.
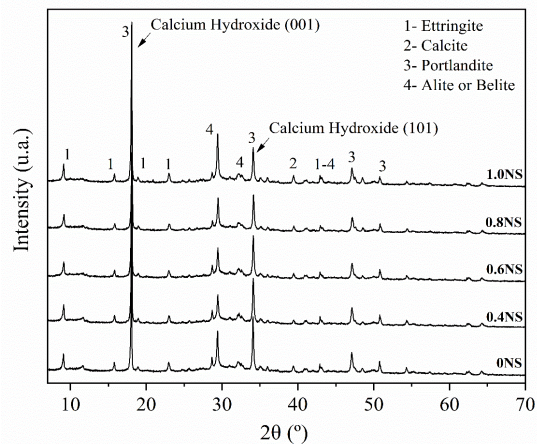
Figure 7. XRD pattern of the cement pastes produced with NS at 28 days of hydration.

4.1.4 FTIR analysis

Figure 8 shows the FTIR spectra of pastes with NS at 28 days. The band at 3640 cm^{-1} is associated with the O-H bound of $Ca(OH)_2$, and at 3444 cm^{-1} is attributed to symmetric and antisymmetric stretching vibrations of water bound present in the phases of C-S-H, monosulfoaluminate, ettringite and/or free water [50]. The greater intensity of the band at 3444 cm^{-1} for 0NS represents a higher amount of free water in that sample. The band at 1650 cm^{-1} corresponds to H-O-H vibrations (also related with free water molecules), there is a decrease for the pastes constituted with NS, confirming the higher formation of C-S-H in these samples when compared with the 0NS paste.

The band of 1430 cm^{-1} is interconnected to the carbonation ratio, higher band intensity means higher carbonation ratio. Lower carbonation is observed with decreasing band intensity, as can be seen for mixtures of 0.4% NS, 0.6% NS, and 1.0% NS [51], [52]. This lower carbonation is related to an increase in the densification of the samples containing NS, which hinders the physical-chemical process of CO_2 ingress into the samples [53].

The band close to 1118 cm^{-1} corresponds to the stretching vibrations of the gypsum and ettringite [50]. The bands of Si-O bond vibrations ($\upsilon3$ 983 cm^{-1} and 875 cm^{-1}, $\upsilon4$ at 514 cm^{-1} and 460 cm^{-1}) were attributed to unreacted C_2S and C_3S and observed for all samples [54], [55]. The band at 460 cm^{-1} is associated with changes in the nature of calcium silicate phases due to SiO_4 polymerization [56]. In general, a reduction in the intensity of Si-O bands is observed with the increase of NS, because of higher C-S-H gel formation.

Rev. IBRACON Estrut. Mater., vol. 15, no. 5, e15509, 2022

9/17
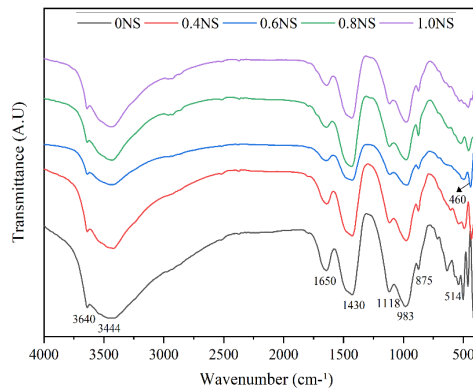
Figure 8. FTIR transmission spectra of cement pastes produced with NS at 28 days.

4.1.5 Compressive strength

The results of compressive strength testing at 28 days of curing are shown in Figure 9. Compared with 0NS, it is possible to see an increase in strength of 55%, 58%, 19%, and 16% for mixtures 0.4NS, 0.6NS, 0.8NS, and 1.0NS, respectively. It is remarkably observed greater compressive strength values to lower NS content, with an optimal strength for 0.6% NS. According to Andrade et al. [41] and Tóbon et al. [21], mixtures with NS show a higher evolution of compressive strength when compared with a paste made only with Portland cement. This is explained by the pozzolanic activity together with the filling effect of this nanomaterial. In other words, NS tends to increase the reaction rate of the mixture, helping in the formation of a higher content of C-S-H during hydration, as well as filling the void between particles of the paste.

For Flores et al. [42] the effect of NS on pastes is even clearer in the early stages, in which there is an increase in compressive strength of up to 116% in the first 8h and 67% at 7 days. According to the results presented previously through the calorimetry test and XRD analysis, pastes with NS reduced the dormant period, released a greater amount of heat in a shorter period, presented a higher total heat released, and consumed a higher anhydrous phase content when compared to the reference paste (0NS). This may indicate a beneficial effect of NS on the compressive strength at 28 days of the evaluated pastes.
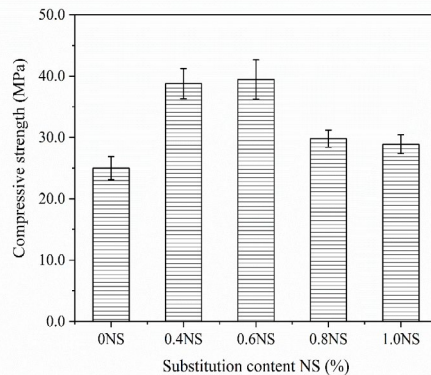
Figure 9. Compressive strength of cement pastes with NS at 28 days.

Therefore, it is possible to conclude that the optimum content of substitution of NS by Portland cement is up to 0.6%. The 0.8% NS and 1.0% NS pastes reached values higher than the reference paste (0NS). This loss of strength for higher NS content pastes may have been caused by the insufficient dispersion of the NS in the mixture, causing an agglomeration of the particles, these results are in according to Nogueira et al. [57].

4.2 Mortars with RFA

Through the pastes results, it was evaluated the effect of recycled fine aggregates (RFA) in mortars containing nanosilica. It was chosen a reference (0% NS) and two replacement levels of Portland cement by NS (0.4% and 0.6% NS) for the manufacture

of mortars with RFA also a blank mixture with standardized sand (REF) was made. The following sections present the results (at 28 days) of the physical-mechanical properties and durability of mortars made of recycled fine aggregate (RFA).

4.2.1 Mechanical properties

The results of the tests on the mechanical properties are shown in Figure 10. Note that all the samples with RFA presented a reduction in strength values (26% of compressive strength in blank mortar) due to the higher porosity (as observed in next section 4.2.2). Higher content of recycled fine aggregate in mortars results in lower strength [6], [58]. There is an increase in compressive strength for the samples containing NS. 0.4NS presented the higher increase in compressive strength (around 56%), however, 0.6NS only improved 6% of compressive strength when compared with 0NS. The gain in compressive strength of NS mortars is directly related to the characteristics of this nanomaterial, since NS provides pozzolanic activity and a great packing capacity of the particles, in order to promote the refinement of the pores [59]. In addition, NS can participate in the hydration process by producing larger amounts of C-S-H due to its accelerated hydration degree provided by the nucleation process, as observed in the paste characterization, increasing the compression strength of mortars. Similar behavior is observed for flexural strength, where a slight increase in strength is observed for NS samples when compared with 0NS.
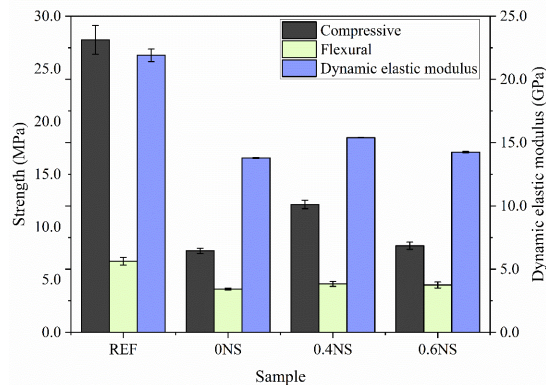
Figure 10. Mechanical properties of mortars produced with RFA and replacement of Portland cement by NS at 28 days.

Erdem et al. [12] found at 28 days that the incorporation of 0.5% to 1.5% of NS in concretes with recycled aggregate increased the mechanical properties with the increase in the NS content. NS enabled an increase in the hydration rate of the cement paste (high Ca/Si ratio at the interface) and in the reactions of pozzolanic activity, constituting a strong connection between the cement mortar and the aggregates.

When compared to the reference, a decrease in compressive strength was expected for mortars composed of 100% RFA. Nonetheless, both samples are classified as category CS iv ($\geq$ 6 MPa) [60], as high strengths are not required for this application. Rendering mortars with a lower strength are less liable to cracking.

In addition, through the results of dynamic elastic modulus, it was observed losses for samples containing RFA, which can be a beneficial factor for mortars, if used for laying and rendering mortars, because the smaller the modulus, the greater the deformation capacity of the mortar, thus, reducing the possibility of cracking in the hardened state.

As observed in the study on pastes, there was an optimal content of nanosilica content. For mortars, this content was 0.4%. The decrease above this value can be associated with lower dispersal ability. The higher absorption and roughness of RFA may have reduced the optimal content of NS in mortars when compared to pastes.

The reduction in the mechanical properties of the RFA compositions can be also attributed to the higher content of SP additive used in the mortar mixtures to obtain the desired spreading. The additive dosage provided greater incorporation of air in the mortars produced, which improved the workability in a fresh state; however, this caused losses in the mechanical properties and influence the reduction of the durability when compared with REF sample.

4.2.2 Capillary water absorption and sorptivity

The results of water absorption by capillarity of mortars with RFA and the blank mixture are shown in Figure 11. The blank mortar (REF) showed the lowest water absorption curve for up to 72 h. In the first 3 h, there was high water

absorption in 0.4NS and 0.6NS mortars. For 0.6NS it was observed that the water absorption produced an increasing curve until 24 h, presenting constant behavior at later ages. 0.4NS absorption presented similar behavior, with a decrease in capillary around 13% during all tests. Compared with the blank mixture, 0NS presented similar early capillary absorption up to 6h of the test, increasing the absorption after this time in up to 25% at 72h.
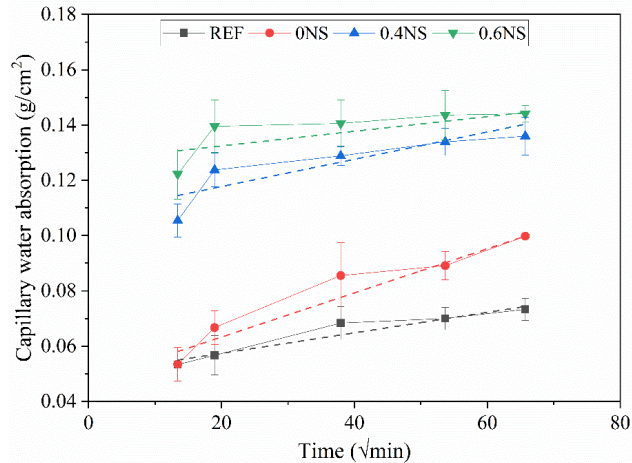
Figure 11. Capillary water absorption of mortars produced with RFA and replacement of Portland cement by NS, at 28 days. Dash lines represents the linear fit.

According to the literature [6], [61], mortars with RFA presents high levels of water absorption by capillarity. This aggregate develops an extremely porous material due to its high water absorption, and particles with high roughness and angularity. This results in an increase in water absorption by capillarity around 50% higher for mortars constituted with the replacement of RFA [6].

Some works identified that the incorporation of NS helps to reduce the absorption of water by capillarity of mortars [14], [15]. This is attributed to the filler and pozzolanic effects, which provide greater pore refinement and filling of empty spaces in the cementitious matrix of the material. After 72 h of testing, Joshaghani et al. [14] obtained a reduction of 14% and 22% for mixtures with 3% NS and 6% NS. Zahedi et al. [15] observed that the reduction of absorption was caused by the larger surface area of the nanoparticles that create more nucleation sites, thus forming a larger amount of C-S-H. In addition, non-reactive particles with $Ca(OH)_2$ crystals can act to fill the voids to further compact the microstructure and reduce the pore volume of the cement paste.

In this research, the mortars containing RFA presented a higher capillary absorption index compared with blank mortar, indicating that these samples are more permeable compared to control. NS provided a higher capillary absorption at the first hours. Three hypotheses were considered for this behavior:

• The mixing process was designed to simplify use on the construction site and did not disperse nanosilica, which was only homogenized with the cement. This may have caused NS agglomeration in the mortar matrix that increased the initial capillary absorption [34].
• A high micropore formation with connected pores, due to the filler effect provided by the nanosilica [62].
• The higher SP content (to achieve the consistency index) resulted in an increase in absorption due to the formation of embedded air bubbles and increased the porosity of the material [63].

The influence of RFA and NS in sorptivity is presented in Table 6. Sorptivity test measures the rate of penetration of water into the mortar pores by capillary suction. To calculate the sorptivity coefficient (S), the cumulative amount of water absorbed per cross sectional area (i) was plotted against the square root of time ($\sqrt{t}$), then the best fit line was obtained by regression analysis and then S was determined from the gradient of the best fit straight line, as presented in Figure 11. It is observed that the presence of RFA increased two times the sorptivity, resulting in a mortar more prominent in water absorption. However, the presence of NS provides an effect in reducing the sorptivity (a decrease of 38% and 67% for 0.4NS and 0.6NS, respectively). It is noticed that even with a lower sorptivity for 0.6NS, the capillarity absorption was higher, suggesting a poor pore refinement. It is concluded that the presence of NS provides a reduction of capillary water absorption even with the higher absorption in the first hours of water contact.

Table 6. Sorptivity coefficient of mortars.

Sample	Sorptivity coefficient		Compressive strength (MPa)
	R^2	Sorptivity (10^{-4} g/cm²/min$^{1/2}$)	
REF	0.95	3.71±0.52	27.76
0NS	0.99	7.98±0.60	7.74
0.4NS	0.76	4.93±1.63	12.13
0.6NS	0.70	2.64±1.04	8.22

4.2.3 Microstructure

Figure 12 shows the microstructure of 0NS and 0.4NS mortars with RFA. For both samples was observed same morphology of hydration products. Figure 12a shows the microstructure of the 0NS, where was identified hydration products as portlandite, ettringite, C-S-H; it is noted that the C–S–H gels remain agglomerated in an 'independent' way, cut and joined by many needle hydrates of ettringite.

For 0.4NS (Figure 12b) lower portlandite formation was observed, with predominant C-S-H amorphous hydration products. 0.4NS mixture achieved greater compressive strength, which can be associated with lower amounts of ettringite needle hydrates and the higher presence of C-S-H amorphous phases. A hypothesis is that the gain in mechanical properties results from C-S-H gel formation, as observed in the EDS presented in Figure 12b, provided by the reaction of NS with portlandite [41]. Higher content of amorphous C-S-H can better fill the internal spaces of the sample. This suggests that the 0.4NS sample became denser and presented a more compact structure, proving the higher values obtained for compressive strength. These results are in line with previous studies [59], [64].
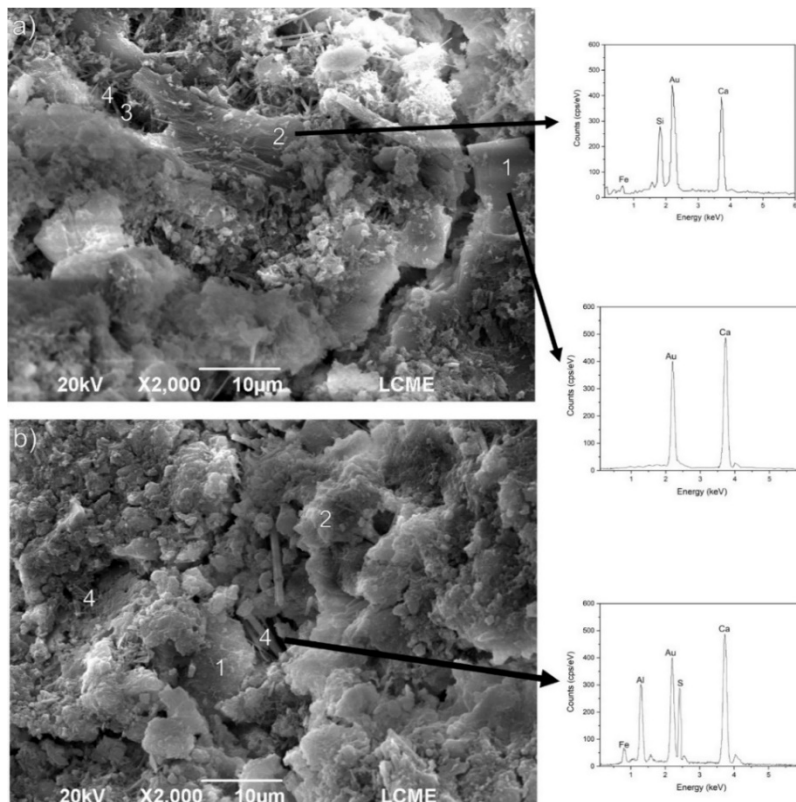
Figure 12. a) SEM images of 0NS and b) 0.4NS at 28 days and correspondent EDS. Legend: 1 = portlandite; 2 = C–S–H; 3 = pore; 4 = ettringite

Rev. IBRACON Estrut. Mater., vol. 15, no. 5, e15509, 2022

13/17

5. CONCLUSIONS

Although nanosilica has a high cost, its use can be offset by replacing natural sand with RFA, in addition to increasing the sustainable appeal of a construction. Based on the results obtained in the present study, the following conclusions can be drawn:

- The NS in its fresh state caused a reduction in the workability of cementitious pastes, i.e., it presented less fluidity than the sample constituted only with Portland cement. As such, it was necessary to use a higher amount of SP to achieve the desired spreading.

- The yield stress and viscosity increased as the replacement content of Portland cement by NS increased. 0.4NS paste reached higher yield stress and shear stress due to a lower dosage of SP in the mixture. 0.6NS and 0.8NS showed similar behavior to the reference sample regarding the results of shear stress/viscosity x shear rate.

- The NS caused an acceleration of the hydration heat in the cementitious matrices, as well as a greater total heat released when compared with the reference paste (0% NS) and increased the formation of hydrated calcium silicate (C-S-H).

- The incorporation of NS provided an increase in compressive strength for all compositions. However, only the low content of nanosilica (0.4NS and 0.6NS) presented the best results.

- RFA showed adequate behavior for the complete replacement of sand in rendering mortars, proving its great environmental benefit. The NS presence contributed to increasing mechanical strength and dynamic modulus. It was possible to observe an improvement of this nanomaterial for mortars with RFA, and the presence of NS provides a reduction of sorptivity and improves the microstructure development.

REFERENCES

[1] A. Akhtar and A. K. Sarmah, "Construction and demolition waste generation and properties of recycled aggregate concrete: A global perspective," *J. Clean. Prod.*, vol. 186, pp. 262–281, 2018, http://dx.doi.org/10.1016/j.jclepro.2018.03.085.

[2] United States Environmental Protection Agency, "Report on the Environmental Protection Agency (EPA)," in *Int. Decontamination Res. and Develop. Conf.*, 2015, EPA/600/R-15/283.

[3] S. W. Tabsh and A. S. Abdelfatah, "Influence of recycled concrete aggregates on strength properties of concrete," *Constr. Build. Mater.*, vol. 23, no. 2, pp. 1163–1167, 2009, http://dx.doi.org/10.1016/j.conbuildmat.2008.06.007.

[4] T. C. F. Oliveira, B. G. S. Dezen, and E. Possan, "Use of concrete fine fraction waste as a replacement of Portland cement," *J. Clean. Prod.*, vol. 273, pp. 123126, 2020, http://dx.doi.org/10.1016/j.jclepro.2020.123126.

[5] A. Bordy, A. Younsi, S. Aggoun, and B. Fiorio, "Cement substitution by a recycled cement paste fine: Role of the residual anhydrous clinker," *Constr. Build. Mater.*, vol. 132, pp. 1–8, 2017, http://dx.doi.org/10.1016/j.conbuildmat.2016.11.080.

[6] T. Gonçalves, R. V. Silva, J. Brito, J. M. Fernández, and A. R. Esquinas, "Mechanical and durability performance of mortars with fine recycled concrete aggregates and reactive magnesium oxide as partial cement replacement," *Cem. Concr. Compos.*, vol. 105, pp. 1–10, 2020, http://dx.doi.org/10.1016/j.cemconcomp.2019.103420.

[7] M. Koushkbaghi, M. J. Kazemi, H. Mosavi, and E. Mohseni, "Acid resistance and durability properties of steel fiber-reinforced concrete incorporating rice husk ash and recycled aggregate," *Constr. Build. Mater.*, vol. 202, pp. 266–275, 2019, http://dx.doi.org/10.1016/j.conbuildmat.2018.12.224.

[8] D. Kong, T. Lei, J. Zheng, C. Ma, J. Jiang, and J. Jiang, "Effect and mechanism of surface-coating pozzalanics materials around aggregate on properties and ITZ microstructure of recycled aggregate concrete," *Constr. Build. Mater.*, vol. 24, no. 5, pp. 701–708, 2010, http://dx.doi.org/10.1016/j.conbuildmat.2009.10.038.

[9] J. Xiao, W. Li, D. J. Corr, and S. P. Shah, "Effects of interfacial transition zones on the stress-strain behavior of modeled recycled aggregate concrete," *Cement Concr. Res.*, vol. 52, pp. 82–99, 2013, http://dx.doi.org/10.1016/j.cemconres.2013.05.004.

[10] R. Wang, N. Yu, and Y. Li, "Methods for improving the microstructure of recycled concrete aggregate: A review," *Constr. Build. Mater.*, vol. 242, 2020, http://dx.doi.org/10.1016/j.conbuildmat.2020.118164.

[11] A. Agarwal, S. Bhusnur, and T. Shanmuga Priya, "Experimental investigation on recycled aggregate with laboratory concrete waste and nano-silica," *Mater. Today Proc.*, vol. 22, pp. 1433–1442, 2019, http://dx.doi.org/10.1016/j.matpr.2020.01.487.

[12] S. Erdem, S. Hanbay, and Z. Güler, "Micromechanical damage analysis and engineering performance of concrete with colloidal nano-silica and demolished concrete aggregates," *Constr. Build. Mater.*, vol. 171, pp. 634–642, 2018, http://dx.doi.org/10.1016/j.conbuildmat.2018.03.197.

[13] J. X. Lu and C. S. Poon, "Improvement of early-age properties for glass-cement mortar by adding nanosilica," *Cement Concr. Compos.*, vol. 89, pp. 18–30, 2018, http://dx.doi.org/10.1016/j.cemconcomp.2018.02.010.

[14] A. Joshaghani and M. A. Moeini, "Evaluating the effects of sugar cane bagasse ash (SCBA) and nanosilica on the mechanical and durability properties of mortar," *Constr. Build. Mater.*, vol. 152, pp. 818–831, 2017, http://dx.doi.org/10.1016/j.conbuildmat.2017.07.041.

[15] M. Zahedi, A. A. Ramezanianpour, and A. M. Ramezanianpour, "Evaluation of the mechanical properties and durability of cement mortars containing nanosilica and rice husk ash under chloride ion penetration," *Constr. Build. Mater.*, vol. 78, pp. 354–361, 2015, http://dx.doi.org/10.1016/j.conbuildmat.2015.01.045.

[16] E. García-Taengua, M. Sonebi, K. M. A. Hossain, M. Lachemi, and J. Khatib, "Effects of the addition of nanosilica on the rheology, hydration and development of the compressive strength of cement mortars," *Compos., Part B Eng.*, vol. 81, pp. 120–129, 2015., http://dx.doi.org/10.1016/j.compositesb.2015.07.009.

[17] I. F. S. Del Bosque, M. Martín-Pastor, S. Martínez-Ramírez, and M. T. Blanco-Varela, "Effect of temperature on C3S and C3S + nanosilica hydration and C - S - H structure," *J. Am. Ceram. Soc.*, vol. 96, no. 3, pp. 957–965, 2013., http://dx.doi.org/10.1111/jace.12093.

[18] P. Hou et al., "Physicochemical effects of nanosilica on C3A/C3S hydration," *J. Am. Ceram. Soc.*, vol. 103, no. 11, pp. 6505–6518, 2020, http://dx.doi.org/10.1111/jace.17364.

[19] G. L. O. Martins, Y. S. B. Fraga, J. S. Vasconcellos, and J. H. João, "Synthesis and characterization of functionalized nanosilica for cementitious composites: review," *J. Nanopart. Res.*, vol. 22, no. 11, 2020, http://dx.doi.org/10.1007/s11051-020-05063-7.

[20] A. Nazari and S. Riahi, "The role of SiO2 nanoparticles and ground granulated blast furnace slag admixtures on physical, thermal and mechanical properties of self compacting concrete," *Mater. Sci. Eng. A*, vol. 528, no. 4–5, pp. 2149–2157, 2011, http://dx.doi.org/10.1016/j.msea.2010.11.064.

[21] J. I. Tobón, J. Payá, and O. J. Restrepo, "Study of durability of Portland cement mortars blended with silica nanoparticles," *Constr. Build. Mater.*, vol. 80, pp. 92–97, 2015, http://dx.doi.org/10.1016/j.conbuildmat.2014.12.074.

[22] Associação Brasileira de Normas Técnicas, *Portland Cement - Requirements,* ABNT NBR 16697 (in Portuguese)," 2018.

[23] American Society for Testing and Materials, *Stand. Specification Portland Cement,* ASTM C150, 2000, http://dx.doi.org/10.1520/C0150.

[24] Associação Brasileira de Normas Técnicas, *Aggregates for concrete - Specification,* ABNT NBR 7211 (in Portuguese), 2009.

[25] Associação Brasileira de Normas Técnicas, *Aggregates - Determination of material finer than 75 um sieve by washing,* ABNT NBR NM 46 (in Portuguese), 2003.

[26] Associação Brasileira de Normas Técnicas, *Fine aggregate - Determination of density and water absorption, ABNT NBR 16916* (in Portuguese), 2021.

[27] Associação Brasileira de Normas Técnicas, *Portland cement - Determination of compressive strength of cylindrical test specimens,* ABNT NBR 7215 (in Portuguese), 2019.

[28] P. Wedding and D. Kantro, "Influence of water-reducing admixtures on properties of cement paste – A miniature slump test," *Cem. Concr. Aggreg.*, vol. 2, no. 2, pp. 95–102, 1980, http://dx.doi.org/10.1520/cca10190j.

[29] C. A. Casagrande, L. F. Jochem, L. Onghero, P. R. Matos, W. L. Repette, and P. J. P. Gleize, "Effect of partial substitution of superplasticizer by silanes in Portland cement pastes," *J. Build. Eng.*, vol. 29, pp. 101226, 2020, http://dx.doi.org/10.1016/j.jobe.2020.101226.

[30] N. H. Azevedo, P. R. Matos, P. J. P. Gleize, and A. M. Betioli, "Effect of thermal treatment of SiC nanowhiskers on rheological, hydration, mechanical and microstructure properties of Portland cement pastes," *Cement Concr. Compos.*, vol. 117, pp. 103903, 2021., http://dx.doi.org/10.1016/j.cemconcomp.2020.103903.

[31] M. Berra, F. Carassiti, T. Mangialardi, A. E. Paolini, and M. Sebastiani, "Effects of nanosilica addition on workability and compressive strength of Portland cement pastes," *Constr. Build. Mater.*, vol. 35, pp. 666–675, 2012., http://dx.doi.org/10.1016/j.conbuildmat.2012.04.132.

[32] C. K. Park, M. H. Noh, and T. H. Park, "Rheological properties of cementitious materials containing mineral admixtures," *Cement Concr. Res.*, vol. 35, no. 5, pp. 842–849, 2005, http://dx.doi.org/10.1016/j.cemconres.2004.11.002.

[33] American Society for Testing and Materials, *Standard Test Method for Compressive Strength of Cylindrical Concrete Specimens,* ASTM C39-21, 2021, http://dx.doi.org/10.1520/C0039.

[34] Y. Sargam and K. Wang, "Influence of dispersants and dispersion on properties of nanosilica modified cement-based materials," *Cement Concr. Compos.*, vol. 118, no. January, pp. 103969, 2021, http://dx.doi.org/10.1016/j.cemconcomp.2021.103969.

[35] Associação Brasileira de Normas Técnicas, *2016 Mortars applied on walls and ceilings - Preparation of mortar mixture for tests*, ABNT NBR 16541, 2016.

[36] Associação Brasileira de Normas Técnicas, *Mortars applied on walls and ceilings - Determination of the consistency index*, ABNT NBR 13276:2016 (in Portuguese), 2016.

[37] Associação Brasileira de Normas Técnicas, *Mortar and hardened concrete — Determination of water absorption by capillarity*, ABNT NBR 9779:2012 (in Portuguese), 2012.

[38] American Society for Testing and Materials, *Standard test method for compressive strength of hydraulic-cement mortars (using portions of prisms broken in flexure)*, ASTM C349-08, 2008, http://dx.doi.org/10.1520/C0349-18.2.

[39] American Society for Testing and Materials, *Standard Test Method for Flexural Strength of Hydraulic-Cement Mortars*, ASTM C348-21, 2021, http://dx.doi.org/10.1520/C0348-21.2.

[40] American Society for Testing and Materials, *Standard Test Method for Dynamic Young's Modulus, Shear Modulus, and Poisson's Ratio by Impulse Excitation of Vibration*, ASTM E1876-15, 2015, http://dx.doi.org/10.1520/E1876-15

[41] D. S. Andrade, J. H. S. Rêgo, P. C. Morais, A. N. M. Lopes, and M. F. Rojas, "Investigation of C-S-H in ternary cement pastes containing nanosilica and highly-reactive supplementary cementitious materials (SCMs): Microstructure and strength," *Constr. Build. Mater.*, vol. 198, pp. 445–455, 2019., http://dx.doi.org/10.1016/j.conbuildmat.2018.10.235.

[42] Y. C. Flores, G. C. Cordeiro, R. D. Toledo Filho, and L. M. Tavares, "Performance of Portland cement pastes containing nano-silica and different types of silica," *Constr. Build. Mater.*, vol. 146, pp. 524–530, 2017., http://dx.doi.org/10.1016/j.conbuildmat.2017.04.069.

[43] L. Silvestro et al., "Influence of ultrasonication of functionalized carbon nanotubes on the rheology, hydration, and compressive strength of portland cement pastes," *Materials*, vol. 14, no. 18, pp. 5248, 2021.

[44] S. Chuah, Z. Pan, J. G. Sanjayan, C. M. Wang, and W. H. Duan, "Nano reinforced cement and concrete composites and new perspective from graphene oxide," *Constr. Build. Mater.*, vol. 73, pp. 113–124, 2014., http://dx.doi.org/10.1016/j.conbuildmat.2014.09.040.

[45] D. Jansen, F. Goetz-Neunhoeffer, B. Lothenbach, and J. Neubauer, "The early hydration of Ordinary Portland Cement (OPC): An approach comparing measured heat flow with calculated heat flow from QXRD," *Cement Concr. Res.*, vol. 42, no. 1, pp. 134–138, 2012., http://dx.doi.org/10.1016/j.cemconres.2011.09.001.

[46] U. Sharma, L. P. Singh, B. Zhan, and C. S. Poon, "Effect of particle size of nanosilica on microstructure of C-S-H and its impact on mechanical strength," *Cement Concr. Compos.*, vol. 97, pp. 312–321, 2019., http://dx.doi.org/10.1016/j.cemconcomp.2019.01.007.

[47] G. Yue, R. Qian-Ping, Y. Xin, C. Cheng, C. Honglei, and L. Kai, "Synthesis of SiO2-PCE core-shell nanoparticles and its modification effects on cement hydration," *Key Eng. Mater.*, vol. 711, pp. 249–255, 2016., http://dx.doi.org/10.1016/j.conbuildmat.2016.03.093.

[48] B. Lothenbach, P. Durdzinski, and K. De Weerdt, *A Practical Guide to Microstrucutral Analysis of Cementitious Materials*. New York: Taylor & Francis Group, 2016.

[49] P. R. Matos, J. S. Andrade, and C. E. M. Campos, "Is the R index accurate to assess the preferred orientation of portlandite in cement pastes," *Constr. Build. Mater.*, vol. 292, pp. 123471, 2021., http://dx.doi.org/10.1016/j.conbuildmat.2021.123471.

[50] B. Yilmaz and A. Olgun, "Studies on cement and mortar containing low-calcium fly ash, limestone, and dolomitic limestone," *Cement Concr. Compos.*, vol. 30, no. 3, pp. 194–201, 2008., http://dx.doi.org/10.1016/j.cemconcomp.2007.07.002.

[51] H. Biricik and N. Sarier, "Comparative study of the characteristics of nano silica-, silica fume- and fly ash-incorporated cement mortars," *Mater. Res.*, vol. 17, no. 3, pp. 570–582, 2014., http://dx.doi.org/10.1590/S1516-14392014005000054.

[52] C. F. Chang and J. W. Chen, "The experimental investigation of concrete carbonation depth," *Cement Concr. Res.*, vol. 36, no. 9, pp. 1760–1767, 2006., http://dx.doi.org/10.1016/j.cemconres.2004.07.025.

[53] Q. Chen, Y. Ke, L. Zhang, M. Tyrer, C. D. Hills, and G. Xue, "Application of accelerated carbonation with a combination of Na2CO3 and CO2 in cement-based solidification/stabilization of heavy metal-bearing sediment," *J. Hazard. Mater.*, vol. 166, no. 1, pp. 421–427, 2009, http://dx.doi.org/10.1016/j.jhazmat.2008.11.067.

[54] T. Vázquez-Moreno and M. T. Blanco-Varela, "Tabla de frecuencias y espectros de absorción infrarroja de compuestos relacionados con la química del cemento," *Mater. Constr.*, vol. 31, no. 182, pp. 31–48, 1981, http://dx.doi.org/10.3989/mc.1981.v31.i182.1007.

[55] N. V. Chukanov and A. D. Chervonnyi, *Infrared Spectroscopy of Minerals and Related Compounds*. Cham: Springer, 2016.

[56] F. Kontoleontos, P. E. Tsakiridis, A. Marinos, V. Kaloidas, and M. Katsioti, "Influence of colloidal nanosilica on ultrafine cement hydration: Physicochemical and microstructural characterization," *Constr. Build. Mater.*, vol. 35, pp. 347–360, 2012, http://dx.doi.org/10.1016/j.conbuildmat.2012.04.022.

[57] G. S. F. Nogueira, N. Schwantes-Cezario, I. C. Souza, C. D. Cavaleiro, M. F. Porto, and B. M. Toralles, "Incorporation of nanosilica in cement composites," *Rev. Mat.*, vol. 23, no. 3, 2018, http://dx.doi.org/10.1590/S1517-707620180003.0516.

[58] G. Santha Kumar, "Influence of fluidity on mechanical and permeation performances of recycled aggregate mortar," *Constr. Build. Mater.*, vol. 213, pp. 404–412, 2019, http://dx.doi.org/10.1016/j.conbuildmat.2019.04.093.

[59] S. Haruehansapong, T. Pulngern, and S. Chucheepsakul, "Effect of the particle size of nanosilica on the compressive strength and the optimum replacement content of cement mortar containing nano-SiO2," *Constr. Build. Mater.*, vol. 50, pp. 471–477, 2014, http://dx.doi.org/10.1016/j.conbuildmat.2013.10.002.

[60] The British Standards, *Specification for Mortar for Masonry Part 1: Rendering and Plastering Mortar,* BS EN 998-1, 2016.

[61] S. K. Kirthika and S. K. Singh, "Durability studies on recycled fine aggregate concrete," *Constr. Build. Mater.*, vol. 250, pp. 118850, 2020, http://dx.doi.org/10.1016/j.conbuildmat.2020.118850.

[62] G. Barluenga, I. Palomar, and J. Puentes, "Hardened properties and microstructure of SCC with mineral additions," *Constr. Build. Mater.*, vol. 94, pp. 728–736, 2015, http://dx.doi.org/10.1016/j.conbuildmat.2015.07.072.

[63] R. C. O. Romano, M. A. Cincotto, and R. G. Pileggi, "Incorporação de ar em materiais cimentícios: uma nova abordagem para o desenvolvimento de argamassas de revestimento," *Ambient. Constr.*, vol. 18, no. 2, pp. 289–308, 2018., http://dx.doi.org/10.1590/s1678-86212018000200255.

[64] H. Li, H. G. Xiao, J. Yuan, and J. Ou, "Microstructure of cement mortar with nano-particles," *Compos., Part B Eng.*, vol. 35, no. 2, pp. 185–189, 2004, http://dx.doi.org/10.1016/S1359-8368(03)00052-0.